TECHNICAL REPORTS

nature neuroscience

Optetrode: a multichannel readout for optogenetic control in freely moving mice

Polina Anikeeva[1,5,6], Aaron S Andalman[1,6], Ilana Witten[1], Melissa Warden[1], Inbal Goshen[1], Logan Grosenick[1], Lisa A Gunaydin[1], Loren M Frank[2] & Karl Deisseroth[1,3,4]

Recent advances in optogenetics have improved the precision with which defined circuit elements can be controlled optically in freely moving mammals; in particular, recombinase-dependent opsin viruses, used with a growing pool of transgenic mice expressing recombinases, allow manipulation of specific cell types. However, although optogenetic control has allowed neural circuits to be manipulated in increasingly powerful ways, combining optogenetic stimulation with simultaneous multichannel electrophysiological readout of isolated units in freely moving mice remains a challenge. We designed and validated the optetrode, a device that allows for colocalized multi-tetrode electrophysiological recording and optical stimulation in freely moving mice. Optetrode manufacture employs a unique optical fiber-centric coaxial design approach that yields a lightweight (2 g), compact and robust device that is suitable for behaving mice. This low-cost device is easy to construct (2.5 h to build without specialized equipment). We found that the drive design produced stable high-quality recordings and continued to do so for at least 6 weeks following implantation. We validated the optetrode by quantifying, for the first time, the response of cells in the medial prefrontal cortex to local optical excitation and inhibition, probing multiple different genetically defined classes of cells in the mouse during open field exploration.

As animal subjects[1], mice provide a very diverse genetic platform for the investigation of behaviors ranging from learning to social performance[2,3], including with optogenetics[4–8]. In particular, viral expression targeting (using promoters or the combination of Cre driver lines[9–12] with Cre-dependent viruses[13–15]) enables highly precise optogenetic investigation of mouse behaviors. However, detailed understanding of effects exerted on neural circuitry has been hindered by the limited ability to simultaneously record multiple channels of electrical activity during optogenetic manipulation in freely moving mice. Researchers have extensively employed electrophysiology both *in vitro* (brain slice and cell culture) and anesthetized *in vivo*[16] to measure the effects of optical stimulation on neural firing. However, the sliced and anesthetized brain differs markedly from the brain in its natural awake state[17]. Thus, neural activity must ideally be observed and perturbed during freely moving behavior to correlate and causally implicate specific neural states with behavioral states.

Although methods for high-throughput awake freely moving electrophysiology are readily available for larger animals such as rats[18–25], combining electrophysiological recordings of multiple isolated units with optical hardware in awake freely moving mice remains a challenge[26] because of the limited size and weight of implants that can be carried by mice. Recently, a number of pioneering efforts have advanced the development of devices for awake electrophysiology in mice, although many of these implants are incompatible with optogenetic approaches[27,28] or require mice to be immobilized and head-fixed during the recording[29] as a result of the dimensions and the weight of the implants. We designed, validated and employed an optetrode, a microdrive optrode, specifically tailored to the constraints and challenges of combining freely moving mouse electrophysiology with optogenetic control.

RESULTS

Optetrode design and validation

Given that optogenetic experimentation fundamentally relies on light delivery into the brain, we began with an optical fiber at the center of the device (**Fig. 1a**). For electrophysiological recordings, the device was equipped with 16 microwires (polymer-coated nickel-chromium alloy, 12-µm diameter) wound into four tetrode bundles[19,20] (diameter, ~25 µm) to facilitate the isolation of signals from individual neurons in the region of light delivery. To ensure consistent and sufficient light intensity near the recording sites, we rigidly attached tetrode bundles to the fiber shaft (diameter, ~200 µm) and cut them to extend 300–1,000 µm beyond the end of the optical fiber. The high fiber diameter to tetrode diameter ratio (200:25) insures negligible shadowing of the light by tetrode bundles. Thus, the fiber acts as both a light source and a structural support for the tetrodes during translation through the brain tissue. The resulting fiber-tetrode assembly was combined with a custom co-axial mechanical drive, thereby allowing the recording site to be manipulated after implantation. The drive design consisted of a vented screw, a thumbnut

[1]Department of Bioengineering, Stanford University, Stanford, California, USA. [2]Department of Physiology, University of California, San Francisco, California, USA. [3]Department of Psychiatry and Behavioral Sciences, Stanford University, Stanford, California, USA. [4]Howard Hughes Medical Institute, Stanford University, Stanford, California, USA. [5]Present address: Department of Materials Science and Engineering, Massachusetts Institute of Technology, Cambridge, Massachusetts, USA. [6]These authors contributed equally to this work. Correspondence should be addressed to K.D. (deissero@stanford.edu).

Received 4 August; accepted 24 October; published online 4 December 2011; corrected online 11 December 2011; doi:10.1038/nn.2992

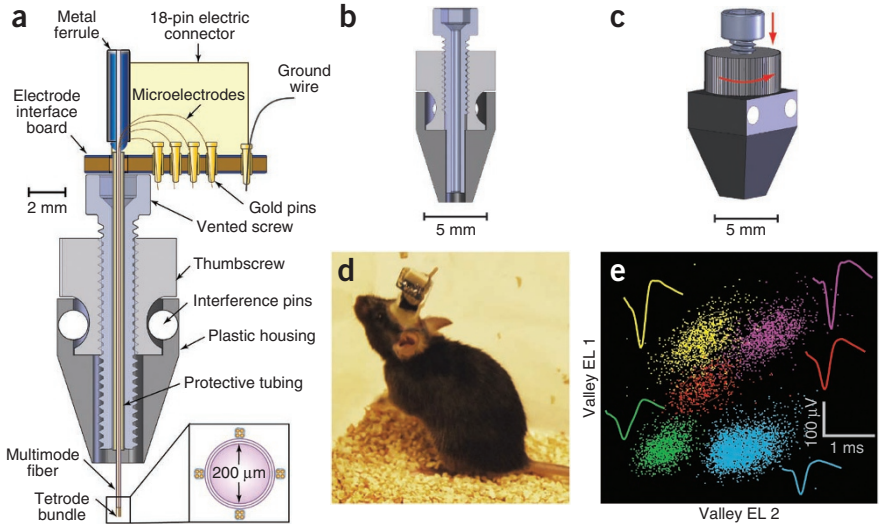

Figure 1 Optetrode design. (**a**) Vertical cross section of the optetrode. The body of the device consists of a plastic housing and a thumbscrew, held tightly in place with two friction-fit plastic pins, mechanically driving a vented screw into which a protective tube containing the four tetrodes and the multimode fiber is glued. The head of the screw is epoxied to both the metal ferrule optical connector end of the fiber and an electronic interface board, which connects the tetrode microwires to an 18-pin electrical connector. Inset, horizontal cross section of the optical fiber with four tetrode bundles affixed. (**b**) Vertical cross section of the mechanical drive perpendicular to the cross section in **a**. The bottom half of the vented screw is thinned such that it tightly fits the tunnel of the plastic housing in only one possible orientation and thus does not rotate during vertical motion. (**c**) Three-dimensional view of the mechanical drive used in the optetrode. As the interference pins prevent the vertical translation of the thumbscrew, turning in the counterclockwise direction results in a downward motion of the vented screw (red arrows). (**d**) Shown is a 10-week-old wild-type male mouse 2 weeks after the optetrode implantation and virus injection (mouse was 8 weeks old at the time of surgery). (**e**) Action potential amplitudes on two channels of a tetrode bundle demonstrate five amplitude clusters (color coded). Average action potential waveforms from the maximum amplitude channel are shown next to each cluster. Unclustered spikes are not shown.

and a plastic housing. The fiber-tetrode assembly ran concentrically through the vented screw, and the vented screw was machined such that the plastic housing prevented its rotation (**Fig. 1b**). Thus, rotation of the thumbnut translated (without rotation) both the screw and the fiber-tetrode assembly co-axially through the brain (**Fig. 1c**; each full turn of the thumbnut corresponded to 454 µm in depth penetration). This mechanical design yielded a combined optical stimulation and electronic recording device (**Fig. 1a**) with a modest weight (2 g on completion and ~2.5 g on implantation, including the weight of the acrylic affixing the device to the scull) and spatial dimensions (height, 22 mm). We found that freely moving adult mice (≥5 weeks old) readily carried the implanted device (**Fig. 1d** and Online Methods).

To test the utility of the optetrode device for awake recording of neural activity, we first implanted the device in the medial prefrontal cortex (mPFC) of mice (n = 3) that were previously injected with adeno-associated virus (AAV5) carrying the gene encoding enhanced yellow fluorescent protein (EYFP). We recorded signals from the 16 microwires as the mice performed an open field exploration task (OFT, see Online Methods). The amplitude of individual spike events measured on each of the four wires of each tetrode formed clusters of amplitude values[18,19] (**Fig. 1e**), and we assessed the quality of these clusters using two standard metrics[30]: L-ratio and isolation distance. Clusters with an L-ratio of less than 0.2 and an isolation distance greater than 15 were deemed single units (see Online Methods; n = 45 single units from 43 OFT experiments, single unit L-ratio = 0.03 ± 0.04, isolation distance = 47.2 ± 24.1, mean ± s.d.). To assess how stable these single units were over the 22-min OFT, we examined how separable the amplitude of spikes from the first 2 min in the OFT were from the amplitude of spikes in the final 2 min. We found that clusters of spikes from the beginning and end of the task were never well-separated from each other (minimum L-ratio = 0.92, mean ± s.d. = 4.9 ± 3.7; maximum isolation distance = 8.2, mean ± s.d. = 4.0 ± 1.4), suggesting that the drive design produces stable recordings. Furthermore, we found that the drive was capable of recording high-quality signals from the same site over a timescale of at least 6 weeks (**Supplementary Fig. 1**).

Recording during optical inhibition in freely moving mice

We next tested to ability of the device to record neural signals in awake behaving mice expressing opsins. To begin, we first investigated performance in mice expressing the halorhodopsin eNpHR3.0, which has been shown to inhibit action potentials during *in vivo* recordings[15], but has not been examined in freely moving mammals. We implanted the device into mice (n = 2) injected with AAV containing the gene encoding eNpHR3.0-EYFP fusion protein under the control of the human *synapsin* promoter (*hSyn*), a broadly expressing neuronal promoter (**Supplementary Fig. 2**). The mice were placed in the open field for 18 min and exposed to 30-s pulses of illumination (λ = 561 nm, continuous light, power density of 160–260 mW mm^{-2} at the tip of the implanted fiber, 17–26 mW mm^{-2} at 0.5 mm and 4–7 mW mm^{-2} at 1 mm below the fiber[31,32]) separated by 90-s dark epochs. We found that, on average, multiunit activity decreased by 26.6 ± 6.8% (mean ± s.d., n = 30 tetrode recording sites across 14 OFTs, $P < 0.001$, t test; **Fig. 2a**) during epochs of illumination. We were able to isolate 23 single units during 14 OFT exposures, and isolation persisted during light exposure in nearly all of the cells (21 of 23 continued to meet cluster quality thresholds during illumination; Online Methods and **Fig. 2b**).

The 21 isolated cells included those in which activity was immediately inhibited (firing rate decreased by 68% ± 15%, mean ± s.d., n = 6 of 21, $z < -1.3$), those in which activity was slowly enhanced, presumably as a result of circuit effects (firing rate increased by 137% ± 56%, mean ± s.d., n = 4 of 21, $z > 1.3$), and those in which no statistically significant effect of light was seen ($P > 0.1$, t test). Of those cells that were affected by light, examination of single neuron firing-rate dynamics before, during and after illumination revealed complex dynamics in response to illumination. Some neurons were robustly and immediately inhibited by light (**Fig. 2c**), some neurons were initially and immediately inhibited by light, but recovered activity over the 30-s illumination epoch (**Fig. 2d**), and other neurons were gradually excited in response to circuit illumination (**Fig. 2e**). These findings demonstrate the potential of the optetrode for capturing the complex changes in neural activity induced by optogenetics in behaving mice, which in this case were induced by the first recording of optogenetic inhibition in a freely moving animal, a long-sought goal.

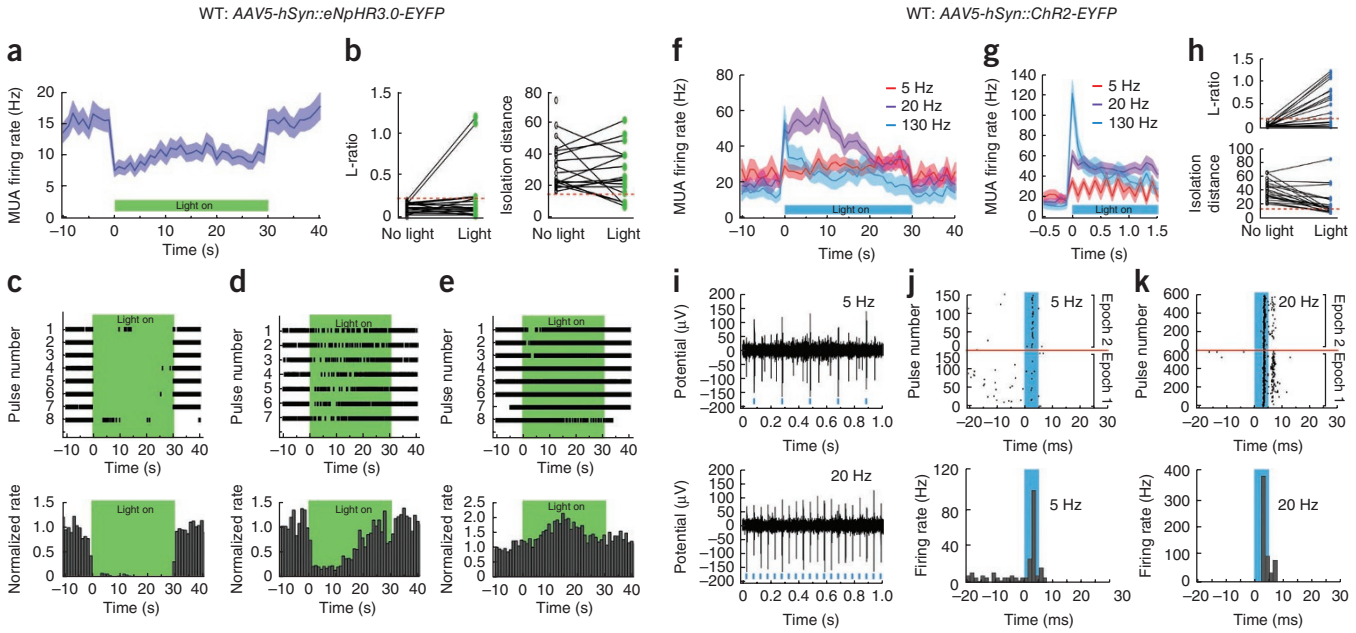

Figure 2 Optetrode-facilitated electrophysiology during broad optogenetic stimulation during the OFT. (**a**–**e**) Wild-type (WT) mice were transduced with *AAV5-hSyn::eNpHR3.0-EYFP*. Average MUA was binned at a rate of 1 Hz (**a**). Shaded area represents s.e.m. ($n = 30$ tetrode recording sites, 14 OFTs). The L-ratio (left) and isolation distance (right) were plotted for the clusters without and during light stimulation ($n = 23$ clusters, **b**). Raster plots (top) and corresponding normalized firing rate profiles (bottom) for are shown for a neuron robustly inhibited by green light (**c**), a neuron initially inhibited by green light, but for which activity recovered over the duration of the stimulation epoch (**d**), and a neuron excited by green light (**e**). (**f**–**k**) Wild-type mice were transduced with *AAV5-hSyn::ChR2-EYFP*. Average MUA was binned at 1 Hz or 10 Hz ($n = 40$ tetrode recording sites, 10 OFTs; **f**,**g**). Shaded area represents s.e.m. The L-ratio (top) and isolation distance (bottom) were plotted for the clusters without and during light stimulation ($n = 21$ clusters, **h**). Examples of a neuron that maintained high cluster quality and coherence with light pulses during 5-Hz (top) and 20-Hz (bottom) stimulation are shown (**i**). Raster plots (top) showing the spike times of the example neuron relative to the onset of each light pulse during 5-Hz and 20-Hz stimulation are shown in **j** and **k**, as well as the corresponding pulse-triggered average firing rates (bottom). Only clusters classified as being well-isolated without light stimulation (see Online Methods) were plotted in **b**–**e** and **h**–**k**. Horizontal dashed lines represent the cut-off for well-isolated clusters.

Recording during optical excitation in freely moving mice

We next explored the integration of electrical recording with optical stimulation over a range of stimulation parameters in freely moving mice. We injected mice ($n = 2$) in mPFC with AAV containing a channelrhodopsin 2 (ChR2)-EYFP fusion protein, again under the control of the *hSyn* promoter, before implanting the optetrode (**Supplementary Fig. 2**). These mice were subjected to an 18-min OFT during which 30-s epochs of optical control were separated by 120-s intervals of no light delivery ($n = 10$ OFTs). The epochs of optical control consisted of pulsed laser light at various frequencies (laser wavelength $\lambda = 473$ nm, pulse width 5 ms, power density 60–160 mW mm^{-2} at the tip of the implanted fiber, corresponding to an estimated power density of 5–12 mW mm^{-2} at 0.5 mm and 1–3 mW mm^{-2} at 1 mm below the fiber, at the tetrode tips). During each OFT, the pulse frequency was twice scanned over the following physiologically and clinically relevant stimulation frequencies: low (5 Hz), moderate (20 Hz) and high (130 Hz; deep brain stimulation[33–35], DBS). These stimulation patterns are commonly delivered from conventional electrodes both in systems neuroscience and in clinical medicine, yet it has proven to be difficult to determine the local neural response to stimulation because of electrical artifacts caused by electrical stimulation, especially at higher frequencies. Although progress has been made understanding the effects of electrical stimulation in head-fixed animals using Ca^{2+} imaging techniques[36], optogenetic stimulation allows us to avoid electrical artifacts and to simultaneously record local neural activity.

We were able to observe multiunit neural response to optical stimulation (**Fig. 2f**), even at 130 Hz. Multiunit activity (MUA, see Online Methods) was significantly increased by 20-Hz stimulation (increased by 115.7 ± 18.6%, mean ± s.d., $n = 40$ tetrode recording sites across 10 OFTs, $P < 0.0001$) and 130-Hz stimulation (37.1 ± 11.7%, mean ± s.d., $P < 0.005$), and began to oscillate with 5-Hz stimulation (MUA binned with finer resolution; **Fig. 2g**). There was a sharp spike in MUA during the first second of 130-Hz stimulation, which subsequently dropped off into a delayed, less excited phase (**Fig. 2g**). This delayed phase was often inhibited and outlasted the period of stimulation, a finding of considerable clinical interest in interpreting DBS mechanisms (**Supplementary Fig. 3**). It was also possible to isolate some single units during stimulation, but increased multiunit background and changes in spike amplitude during ChR2-facilitated light stimulation made isolation difficult for many units. This was reflected in decreased cluster quality metrics during stimulation (**Fig. 2h**). Nonetheless, many units remained well-isolated during stimulation (9 of 21 units, 10 OFTs; **Fig. 2i**–**k** and **Supplementary Fig. 4**).

One possible explanation for some of the reduced number of well-isolated single units during ChR2-mediated stimulation is that the *ChR2* gene was driven by the broadly expressing *hSyn* promoter[37]. By testing the optetrode in mice expressing ChR2 in more specific populations of neurons (also more concordant with how optogenetics will typically be used in combination with the optetrode), we hypothesized that we could improve cluster quality during optical stimulation. We implanted the optetrode drive into two additional classes of mice: mice expressing ChR2 under a more specific promoter (*CaMKIIα*) and mice expressing ChR2 in a recombinase-dependent targeted manner in parvalbumin-expressing neurons (*PV::Cre* transgenic line); in both cases, we injected AAV5 into the mPFC as in the previous experiments (**Supplementary Figs. 5** and **6**).

We subjected mice injected with *AAV5-CaMKIIα::ChR2-EYFP* into mPFC ($n = 2$) to a 22-min OFT using an experimental protocol identical to that used for the *hSyn* mice, but with an additional 130-Hz stimulation epoch using a 2-ms pulse width instead of 5 ms. This additional epoch was intended to decrease the duty cycle of the high-frequency stimulation, in a procedure that is more relevant to clinical DBS. We also randomized the order of the various stimulation frequencies (laser wavelength $\lambda = 473$ nm, power density = 96 mW mm^{-2} at the tip of the implanted fiber, corresponding to an estimated power density of 9 mW mm^{-2} at 0.5 mm and 2 mW mm^{-2} at 1 mm below the fiber, at the tetrode tips). Again, we observed increased MUA during 20-Hz stimulation (173% increase, $n = 84$ tetrode recording sites across 33 OFTs; **Fig. 3a**) and oscillatory MUA during 5-Hz stimulation (**Fig. 3b**). We found no significant change in MUA at any stimulation frequency in *CaMKIIα::EYFP* ($P > 0.2$). However, in contrast with the *hSyn* promoter, the 130-Hz response did not decrease to baseline following the initial peak in mice expressing ChR2 under the control of the *CaMKIIα* promoter (**Fig. 3a**). The cluster quality for isolated neurons changed during light stimulation (7 of 14 units remained isolated, $n = 33$ OFTs; **Fig. 3c**), but robust responses to individual light pulses could be observed in the cells that remained isolated (for example, latency = 4.9 ± 0.3 ms, mean ± s.d.; **Fig. 3d–f**).

To further explore the ability of the optetrode to isolate individual neurons during ChR2-driven optical excitation, we explored the effects of stimulation of a sparse neuronal population of inhibitory interneurons, namely parvalbumin-expressing cells. We again implanted optetrodes in mPFC; however, instead of using wild-type mice, we injected *PV::Cre* mice ($n = 2$)[38] with AAV5 carrying a *loxP*-flanked ChR2-EYFP fusion construct (DIO) under the control of the *EF1α* promoter[13,14]. The DIO construct allows for the protein of interest to be expressed only in the cells that express Cre recombinase (**Supplementary Fig. 6**). We subjected the mice to an OFT protocol identical to that used for mice expressing *CaMKIIα::ChR2* and recorded local MUA (**Fig. 3g**) and single unit activity. In this case, the ability to maintain high cluster quality was nearly unaffected by light stimulation (**Fig. 3h**), allowing almost all of the single units that were isolated to be observed during light stimulation ($n = 46$ of 50 single units over 29 OFTs; **Fig. 3h**, see Online Methods). Notably, in this case, we observed little effect on mean MUA during light stimulation in these mice (**Fig. 3g**), but individual units (**Fig. 3i**) showed robust responses, such as transient inhibition, to individual light pulses (**Fig. 3j**,**k** and **Supplementary Fig. 7**). None of these units displayed low-jitter action potentials in response to light, suggesting they were not ChR2-expressing parvalbumin-positive neurons. Instead, a significant number of units showed a broad and delayed inhibition in response to light ($P < 0.0005$, binomial test; 9 of 46 neurons show reduced firing rate, $P < 0.05$, Bonferroni corrected t test; **Fig. 3j**,**k**), as might be expected from synaptic or multisynaptic effects of successfully recruiting parvalbumin-positive[14] neuronal activity. Indeed, no neurons recorded in parvalbumin-positive EYFP control mice showed a change in firing rate in response to light ($n = 3$ mice, 0 of 29 neurons, $P > 0.05$; Online Methods).

Mouse behavior during optical excitation

A critical feature of the optetrode drive design is that it remains small and light enough to be used in freely behaving mice. We were

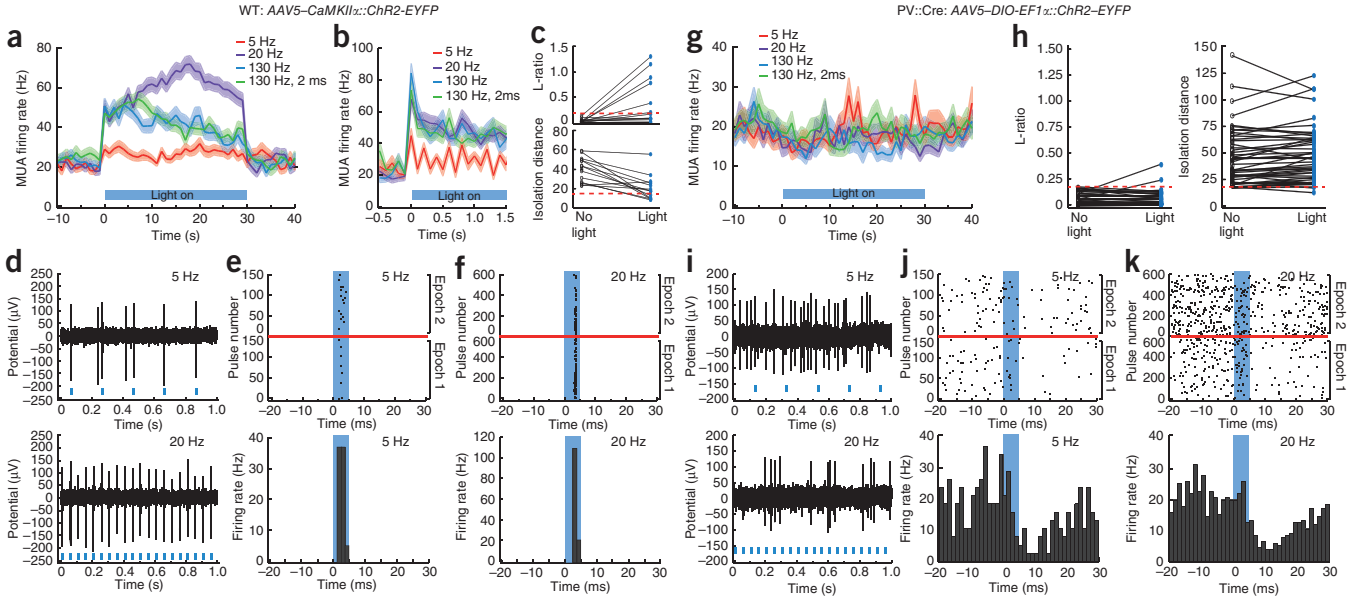

Figure 3 Optetrode-facilitated electrophysiology during cell type–specific optogenetic stimulation in the context of the OFT. (**a**–**f**) Wild-type mice were transduced with *AAV5-CaMKIIα::ChR2-EYFP*. Average MUA was binned at a rate of 1 Hz (**a**) and 10 Hz (**b**). Shaded areas represent s.e.m. ($n = 84$ tetrode recording sites, 33 OFTs). The L-ratio (top) and isolation distance (bottom) were plotted for clusters without and during light stimulation ($n = 14$ clusters, **c**). An example neuron is shown that maintained high cluster quality and coherence with light pulses during 5-Hz (left) and 20-Hz (right) optical stimulation (**d**). Raster plots of spike times (left) and pulse-triggered average firing rates (right) are shown for an example neuron relative to the onset of each light pulse during 5-Hz (**e**) and 20-Hz (**f**) stimulation. (**g**–**k**) *PV::Cre* transgenic mice were transduced with *AAV5–DIO-EF1α::ChR2-EYFP*. Average MUA was binned at 1 Hz (**g**). Shaded areas represent s.e.m. ($n = 45$ tetrode recording sites, 29 OFTs). The L-ratio (left) and isolation distance (right) were plotted without and during light stimulation ($n = 50$ clusters, **h**). An example neuron is shown that maintained high cluster quality and decreased firing rate in response to 5-Hz (left) and 20-Hz (right) stimulation of parvalbumin-expressing cells (**i**). Raster plots of spike times (left) and pulse-triggered average firing rates (right) are shown for the example neuron relative to the onset of each light pulse during 5-Hz (**j**) and 20-Hz (**k**) stimulation. Only clusters classified as well-isolated without light stimulation (see Online Methods) were plotted in **c**–**f** and **h**–**k**. Horizontal dashed lines represent cut-off for well-isolated clusters.

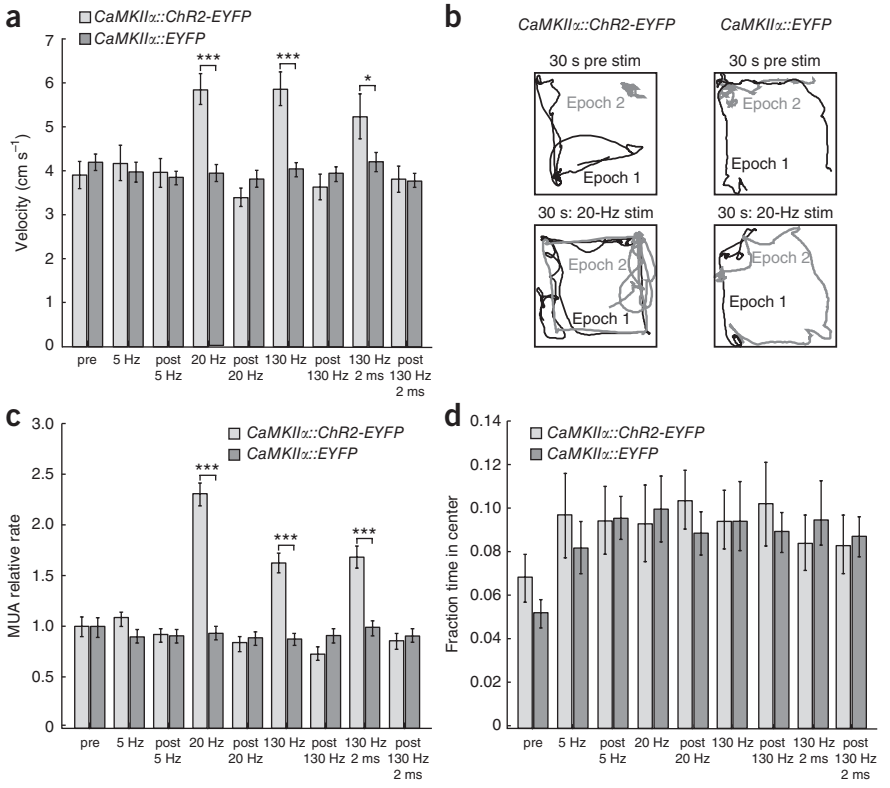

Figure 4 Behavioral and neural activity effects of optogenetic stimulation during the OFT. Mice were subjected to a 22-min OFT and were exposed to 30-s light stimulation epochs every 2 min. We used 5 Hz, 20 Hz, 130 Hz with 5-ms pulse width and 130 Hz with 2-ms pulse width for stimulation parameters. Each stimulation type was used exactly twice and the order was randomized. (**a**) Velocity of *CaMKIIα::ChR2-EYFP* ($n = 84$ tetrode recording sites across 33 OFTs in 2 mice) and *CaMKIIα::EYFP* mice ($n = 119$ tetrode recording sites across 43 OFTs in 3 mice) in mPFC during and after each stimulation epoch. $^{*}P < 0.05$, $^{***}P < 0.001$. (**b**) Example OFT traces showing the path of the mice during the 30 s immediately before stimulation (top) and then during 30 s of 20-Hz stimulation (bottom). (**c**,**d**) Data are presented as in **a** for normalized average multi-unit firing rate (**c**) and the percent time spent in the center of the open field (**d**). All error bars indicate s.e.m.

able to simultaneously explore the effects of optical stimulation in the mPFC on both neural activity and behavior in the OFT. We analyzed two aspects of the behavior during the 22-min OFT: mouse velocity and the periods of time during which mice occupied the center of the cage, a validated measure of anxiety-related behaviors[39]. We calculated the average velocity prior to the first optical stimulation epoch, as well as during and after different frequency and pulse-width stimulation epochs, for each OFT. Notably, we found that mice expressing ChR2 in excitatory neurons (*CaMKIIα::ChR2*) showed increased velocity during 20-Hz and 130-Hz stimulation ($P < 0.0001$ for 20 and 130 Hz, 5-ms pulse width stimulation; $P < 0.02$ for 130 Hz, 2-ms pulse width; Bonferroni corrected t test; **Fig. 4a**) and thus had longer path lengths during stimulation (**Fig. 4b**), but this increase did not occur during 5-Hz stimulation. This pattern is consistent with the frequencies of stimulation that produced increased MUA

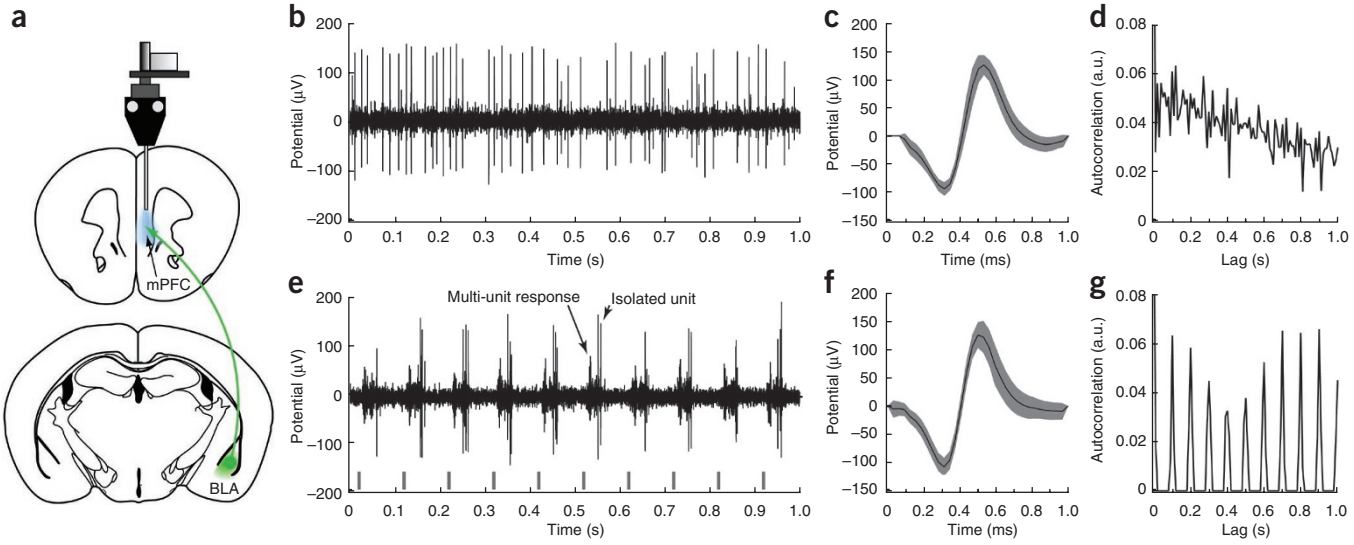

Figure 5 Optetrode projection targeting: driving axonal inputs from BLA into mPFC. (**a**) Schematic showing BLA-to-mPFC projection targeting. (**b**) Spontaneous activity of a PrL neuron is shown over a 1-s time window. (**c**) Average action potential shape is shown for the recording in **b**. Shaded area indicates the s.e.m. from the mean. (**d**) Autocorrelation analysis of the firing rate of the unit in **b** revealed no clear periodicity of the firing pattern on the scale of ≤1 s. a.u., arbitrary units. (**e**) Light stimulation of the BLA-to-mPFC projection evoked action potentials of the unit in **b** and also a complex multi-unit response (data not shown). (**f**) Average action potential shape is shown for the recording in **e**. (**g**) Autocorrelation analysis revealed that the unit fired with periodicity of 10 Hz coherent with applied optical stimulation during freely moving open field exploration. Laser light was employed at λ = 473 nm, 5-ms pulse width, 10-Hz rate and power density of 80 mW mm^{-2} at the tip of the implanted fiber (6 mW mm^{-2} at 0.5 mm and 1 mW mm^{-2} at 1 mm below the fiber, at the tetrode tips).

(**Fig. 4c**). EYFP no-opsin controls, on the other hand, did not exhibit any effects of light on average MUA or velocity. Previous studies[16,40] observed locomotion changes with cortical optical stimulation, but, crucially, were unable to provide information on local neuronal activity during the observed behavioral effect; with the optetrode, this information is available.

To quantify the time spent in the center of the open field, we computed the fraction of each epoch during which the mouse was more than 10 cm from the closest side of the open field box. We found that the light-stimulation procedure had no mean effect on the time that the *CaMKIIα::ChR2* mice spent in the center of the open field as compared to the *CaMKIIα::EYFP* control mice ($P > 0.1$; **Fig. 4d**), although both types of mice spent less time in the center during their initial 2-min pre-stimulation period than they did in subsequent periods, suggesting a natural acclimation to the field ($P < 0.05$; **Fig. 4d**). We carried out the same analyses for mice expressing ChR2 in parvalbumin-positive cells, and we did not observe mean effects of optical stimulation on animal velocity, time spent in the center or recorded MUA (**Supplementary Fig. 8**).

Recording of defined neural projections in freely moving mice

The optetrode method need not be limited to recording activity in the region containing opsin-expressing cell bodies, but could, in principle, be extended to recording from cells that receive projections from a remote brain region transduced with an opsin. In a final set of experiments, we tested the capabilities of the optetrode for driving specific neural projections between brain areas and assessing the functional effects of those projections in freely moving mice. We injected an AAV5 encoding ChR2-EYFP under the control of the *CaMKIIα* promoter into the basolateral amygdala (BLA), but did not implant the optetrode in the BLA, instead placing the optetrode above the prelimbic (PrL) neocortex. In this case the activity of PrL neurons could be recorded while stimulating the projection from the BLA to the mPFC[41], of which PrL is a part (**Fig. 5a**). This projection-targeting strategy is feasible for opsins that traffic well to axons[6,15,16].

The background activity of a PrL unit (**Fig. 5b**,**c**) showed no underlying periodicity in its firing pattern (**Fig. 5d**). However, when 10-Hz stimulation with blue light ($\lambda = 473$ nm) was used to drive the BLA projection into mPFC, the isolated unit showed a marked change in temporal patterning (**Fig. 5e**), maintaining the same spike waveform (**Fig. 5f**). The autocorrelation of the recording of this unit during optical projection stimulation revealed a 0.1-s periodicity, consistent with 10-Hz stimulation (**Fig. 5g**). In addition to the synchronization of the single unit with the laser pulses, the stimulation also produced complex multiunit responses that preceded (but did not impair isolation of) synchronous firing of the observed unit (data not shown) in these freely behaving mice.

DISCUSSION

Combining the precision of optogenetic control with electrophysiological readout of single-unit neural dynamics is essential for behavioral experiments seeking to establish causality and deepen the understanding of neural circuit dynamics. We have developed an optrode device, the optetrode, that allows for simultaneous optical interrogation and tetrode electrophysiology in awake freely moving mice. A key feature of the optetrode is its fiber-centric design that allows the use of a single-screw drive for propagation of the optical fiber and tetrodes over a 4-mm range of brain depths (**Fig. 1a**–**c**). This mechanical drive design reduces the dimensions and weight of the device and allows it to be comfortably carried by a freely moving mouse. We and others have recently demonstrated[42,43] integration of optogenetic control and multiunit recording in behaving mice, but have lacked the capability to co-advance the light source and the recording electrodes together in a fixed and predictable spatial relationship through multiple brain regions in the same animal; indeed, the optical fiber in the optetrode also doubles as a structural support for the tetrodes, allowing accurate and robust targeting of deep brain structures. Moreover, the optetrode integrates freely moving mouse electrophysiology with optogenetics at a low cost and with a straightforward fabrication procedure that does not require a specialized facility.

We validated the optetrode by quantifying for the first time, to the best of our knowledge, the physiological effects of optical inhibition or excitation of defined local mPFC cells in freely moving mice. The observed robust inhibition of neural activity via eNpHR3.0 activation (**Fig. 2a**) was expected from the mechanism of operation of halorhodopsin. However, the optetrode's ability to record the activity of individual neurons during light stimulation (**Fig. 2b**) revealed the diversity of the responses in the local network (**Fig. 2c**–**e**). It is likely that the neurons that were inhibited in an immediate and sustained manner by light (**Fig. 2c**) expressed eNpHR3.0, and their firing responses were dominated by the eNpHR3.0-mediated chloride currents. In contrast, the neurons that displayed higher firing rates during illumination (**Fig. 2e**) likely received inputs from inhibitory neurons that normally suppress their activity, but are inhibited by light. Thus, the firing dynamics of these neurons are only indirectly influenced by the eNpHR3.0 response to light. Similarly, the initial rapid (<100 ms) decrease of the firing rate of many units (**Fig. 2d**) on illumination is probably a consequence of eNpHR3.0 expression and function, but, subsequent dynamics that do not match eNpHR3.0 dynamics may be governed by network activity. Notably, we found that neurons that were inhibited displayed a very rapid time course of inhibition onset that was consistent with the known fast-pumping mechanism. This finding supports a direct and cell-intrinsic mode of optogenetic inhibition in these mammalian preparations. As with optogenetic excitation, identifying these properties in freely moving mice would be difficult without simultaneous multichannel readout during optogenetic manipulation.

Resolution of individual neurons during ChR2-facilitated pulsed blue-light excitation was, as expected, dependent on the density of photosensitive cells. In the dense population of ChR2-expressing cells resulting from the use of either the *hSyn* or *CaMKIIα* promoters to drive expression in mPFC, the coherent population response to pulsed stimulation often overwhelmed the responses of individual units (**Figs. 2h** and **3c**). However, many of the units still retained high cluster quality while exhibiting high coherence with stimulation pulses (**Figs. 2i**–**k** and **3d**–**f**). In contrast, cluster quality and the ability to isolate individual units were unaffected during light stimulation of a local network containing a reduced density of ChR2-expressing cells, as with parvalbumin-expressing neurons (**Fig. 3i**), a typical setting for optogenetic experiments. In such a setting, the optetrode has clear advantages over recording during electrical stimulation, with which electrical artifacts limit resolution and cell type–specific stimulation is not possible.

Our observation of the dynamic changes of the electrophysiological response to 130-Hz stimulation (**Figs. 2f**,**g** and **3a**,**b** and **Supplementary Fig. 7**) over the course of 30-s stimulation epochs not only improves our understanding of DBS strategies that employ these frequencies (although it is important to note that DBS electrodes may recruit a different pattern of axons and cell bodies than optogenetic stimulation), but also highlights the importance of electrophysiological recordings during optogenetic behavioral

experiments, as it is especially difficult to resolve effects on local circuitry when using electrical DBS because of electrical artifacts. In addition to providing insight into network activity during optogenetic stimulation of local somata, the optetrode can be used to provide a readout of neural activity affected by stimulation of specific projections (**Fig. 5**). Finally, because of its modest weight and footprint (0.12 mm^2 at the site of implantation and 8 mm^2 on the surface of the skull), the optetrode can be combined with other sources of stimulation, such as optical fibers, or additional recording electrodes in contributing to the increasingly rich toolbox for neural circuit interrogation.

As the optetrode can be easily fabricated at low cost (<$100) without specialized equipment and minimal training (**Supplementary Note** and **Supplementary Fig. 9**) and provides high-quality electrophysiological recordings during behavioral experiments, it becomes straightforward to routinely supplement transduced animal cohorts with optetrode-implanted animals that can be used to monitor units during optogenetically driven behavior. This approach will facilitate the analysis of behavioral data, reducing the number of interpretations to those consistent with observed (rather than hypothesized) local unit activity and thereby minimizing biases and preconceptions in the analysis of mouse behavior. By providing a fast multichannel readout compatible with the speed and specificity of optogenetics, the optetrode takes a step toward furthering the development of precise and causal circuit interrogation for systems neuroscience.

METHODS

Methods and any associated references are available in the online version of the paper at http://www.nature.com/natureneuroscience/.

Note: Supplementary information is available on the Nature Neuroscience website.

ACKNOWLEDGMENTS

We thank S. Arber for the *PV::Cre* transgenic mouse line. P.A. thanks D.G. Walker for advice on mechanical design. P.A. was supported by a Dean's fellowship from Stanford University School of Medicine, I.W. was supported by the Helen Hay Whitney Foundation, I.G. was supported by a Machiah fellowship and the Weizmann Institute Women in Science award, L.G. was supported by a National Science Foundation Integrative Graduate Education and Research Traineeship Award, and L.A.G. was supported by a BioX fellowship from Stanford University. L.M.F. and K.D. received support from a GO grant from the National Institute of Neurological Disorders and Stroke. Full funding information for K.D. is listed at http://www.stanford.edu/group/dlab/optogenetics/funding/ and includes the Gatsby Charitable Foundation, the Defense Advanced Research Projects Agency Reorganization and Plasticity to Accelerate Injury Recovery Program, the California Institute for Regenerative Medicine, the McKnight Foundation, the National Institute of Mental Health, and the National Institute on Drug Abuse.

AUTHOR CONTRIBUTIONS

P.A., A.S.A. and K.D. designed the experiments and analyzed the data. P.A. devised and designed the device. P.A. and A.S.A. collected and analyzed electrophysiological and behavioral data. P.A., A.S.A. and I.G. performed immunohistochemical processing and confocal imaging. M.W. and I.W. aided in the development of the device and surgical procedure. M.W. and L.M.F. aided with neuronal sorting procedures. L.G. aided in statistical analysis. L.A.G. contributed data regarding defined-projection manipulation. L.M.F. aided the analysis of the electrophysiological data. K.D. supervised all aspects of the work. P.A., A.S.A. and K.D. wrote the paper.

COMPETING FINANCIAL INTERESTS

The authors declare no competing financial interests.

Published online at http://www.nature.com/natureneuroscience/.
Reprints and permissions information is available online at http://www.nature.com/reprints/index.html.

1. Nestler, E.J. & Hyman, S.E. Animal models of neuropsychiatric disorders. *Nat. Neurosci.* **13**, 1161–1169 (2010).
2. Costa, R.M. *et al.* Mechanism for the learning deficits in a mouse model of neurofibromatosis type 1. *Nature* **415**, 526–530 (2002).
3. Leypold, B.G. *et al.* Altered sexual and social behaviors in trp2 mutant mice. *Proc. Natl. Acad. Sci. USA* **99**, 6376–6381 (2002).
4. Boyden, E.S., Zhang, F., Bamberg, E., Nagel, G. & Deisseroth, K. Millisecond-timescale, genetically targeted optical control of neural activity. *Nat. Neurosci.* **8**, 1263–1268 (2005).
5. Zhang, F. *et al.* Multimodal fast optical interrogation of neural circuitry. *Nature* **446**, 633–639 (2007).
6. Petreanu, L., Huber, D., Sobczyk, A. & Svoboda, K. Channelrhodopsin-2–assisted circuit mapping of long-range callosal projections. *Nat. Neurosci.* **10**, 663–668 (2007).
7. Adamantidis, A.R., Zhang, F., Aravanis, A.M., Deisseroth, K. & de Lecea, L. Neural substrates of awakening probed with optogenetic control of hypocretin neurons. *Nature* **450**, 420–424 (2007).
8. Arenkiel, B.R. *et al. In vivo* light-induced activation of neural circuitry in transgenic mice expressing channelrhodopsin-2. *Neuron* **54**, 205–218 (2007).
9. Huang, Z.J., Yu, W., Lovett, C. & Tonegawa, S. Cre/*loxP* recombination-activated neuronal markers in mouse neocortex and hippocampus. *Genesis* **32**, 209–217 (2002).
10. Lindeberg, J. *et al.* Transgenic expression of Cre recombinase from the tyrosine hydroxylase locus. *Genesis* **40**, 67–73 (2004).
11. Gong, S. *et al.* Targeting Cre recombinase to specific neuron populations with bacterial artificial chromosome constructs. *J. Neurosci.* **27**, 9817–9823 (2007).
12. Young, P. *et al.* Single-neuron labeling with inducible Cre-mediated knockout in transgenic mice. *Nat. Neurosci.* **11**, 721–728 (2008).
13. Tsai, H.C. *et al.* Phasic firing in dopaminergic neurons is sufficient for behavioral conditioning. *Science* **324**, 1080–1084 (2009).
14. Sohal, V.S., Zhang, F., Yizhar, O. & Deisseroth, K. Parvalbumin neurons and gamma rhythms enhance cortical circuit performance. *Nature* **459**, 698–702 (2009).
15. Gradinaru, V. *et al.* Molecular and cellular approaches for diversifying and extending optogenetics. *Cell* **141**, 154–165 (2010).
16. Gradinaru, V. *et al.* Targeting and readout strategies for fast optical neural control *in vitro* and *in vivo*. *J. Neurosci.* **27**, 14231–14238 (2007).
17. Brown, E.N., Purdon, P.L. & Van Dort, C.J. General anesthesia and altered states of arousal: a systems neuroscience analysis. *Annu. Rev. Neurosci.* **34**, 601–628 (2011).
18. McNaughton, B.L., O'Keefe, J. & Barnes, C.A. The stereotrode: a new technique for simultaneous isolation of several single units in the central nervous system from multiple unit records. *J. Neurosci. Methods* **8**, 391–397 (1983).
19. Wilson, M.A. & McNaughton, B.L. Dynamics of the hippocampal ensemble code for space. *Science* **261**, 1055–1058 (1993).
20. Gray, C.M., Maldonado, P.E., Wilson, M. & McNaughton, B.L.J. Tetrodes markedly improve the reliability and yield of multiple single-unit isolation from multi-unit recordings in cat striate cortex. *J. Neurosci. Methods* **63**, 43–54 (1995).
21. Jog, M.S. *et al.* Tetrode technology: advances in implantable hardware, neuroimaging, and data analysis techniques. *J. Neurosci. Methods* **117**, 141–152 (2002).
22. Nakazawa, K. *et al.* Requirement for hippocampal CA3 NMDA receptors in associative memory recall. *Science* **297**, 211–218 (2002).
23. Wiltgen, B.J., Brown, R.A., Talton, L.E. & Silva, A.J. New circuits for old memories: the role of the neocortex in consolidation. *Neuron* **44**, 101–108 (2004).
24. Chawla, M.K. & Barnes, C.A. Hippocampal granule cells in normal aging: insights from electrophysiological and functional imaging experiments. *Prog. Brain Res.* **163**, 661–678 (2007).
25. Gerrard, J.L., Burke, S.N., McNaughton, B.L. & Barnes, C.A. Sequence reactivation in the hippocampus is impaired in aged rats. *J. Neurosci.* **28**, 7883–7890 (2008).
26. Scanziani, M. & Häusser, M. Electrophysiology in the age of light. *Nature* **461**, 930–939 (2009).
27. McHugh, T.J., Blum, K.I., Tsien, J.Z., Tonegawa, S. & Wilson, M.A. Impaired hippocampal representation of space in CA1-specific NMDAR1 knockout mice. *Cell* **87**, 1339–1349 (1996).
28. Jeantet, Y. & Cho, Y.H. Design of a twin tetrode microdrive and headstage for hippocampal single unit recordings in behaving mice. *J. Neurosci. Methods* **129**, 129–134 (2003).
29. Royer, S. *et al.* Multi-array silicon probes with integrated optical fibers: light-assisted perturbation and recording of local neural circuits in the behaving animal. *Eur. J. Neurosci.* **31**, 2279–2291 (2010).
30. Schmitzer-Tobert, N., Jackson, J., Henze, D., Harris, K. & Redish, A.D. Quantitative measures of cluster quality for use in extracellular recordings. *Neuroscience* **131**, 1–11 (2005).
31. Aravanis, A.M. *et al.* An optical neural interface: *in vivo* control of rodent motor cortex with integrated fiberoptic and optogenetic technology. *J. Neural Eng.* **4**, S143–S156 (2007).
32. Diester, I. *et al.* An optogenetic toolbox designed for primates. *Nat. Neurosci.* **14**, 387–397 (2011).
33. Benabid, A.L., Chabardes, S., Mitrofanis, J. & Pollak, P. Deep brain stimulation of the subthalamic nucleus for the treatment of Parkinson's disease. *Lancet Neurol.* **8**, 67–81 (2009).
34. Ponce, F.A. & Lozano, A.M. Deep brain stimulation state of the art and novel stimulation targets. *Prog. Brain Res.* **184**, 311–324 (2010).

35. Mayberg, H.S. Targeted electrode-based modulation of neural circuits for depression. *J. Clin. Invest.* **119**, 717–725 (2009).
36. Histed, M.H., Bonin, V. & Reid, R.C. Direct activation of sparse, distributed populations of cortical neurons by electrical microstimulation. *Neuron* **63**, 508–522 (2009).
37. Thiel, G., Greengard, P. & Südhof, T.C. Characterization of tissue-specific transcription by the human synapsin I gene promoter. *Proc. Natl. Acad. Sci. USA* **88**, 3431–3435 (1991).
38. Hippenmeyer, S. *et al.* A Developmental switch in the response of DRG neurons to ETS transcription factor signaling. *PLoS Biol.* **3**, e159 (2005).
39. Britton, D.R. & Britton, K.T. A sensitive open field measure of anxiolytic drug activity. *Pharmacol. Biochem. Behav.* **15**, 577–582 (1981).
40. Gradinaru, V., Mogri, M., Thompson, K.R., Henderson, J.M. & Deisseroth, K. Optical deconstruction of parkinsonian neural circuitry. *Science* **324**, 354–359 (2009).
41. Bacon, S.J., Headlam, A.J., Gabbott, P.L. & Smith, A.D. Amygdala input to medial prefrontal cortex (mPFC) in the rat: a light and electron microscope study. *Brain Res.* **720**, 211–219 (1996).
42. Yizhar, O. *et al.* Neocortical excitation-inhibition balance in information processing and social dysfunction. *Nature* **477**, 171–178 (2011).
43. Halassa, M.M. *et al.* Selective optical drive of thalamic reticular nucleus generates thalamic bursts and cortical spindles. *Nat. Neurosci.* **14**, 1118–1120 (2011).

ONLINE METHODS

Optetrode fabrication. We attached 16 polymer-coated NiCr microwires (PF000591, Kanthal Palm Coast) to an electrode interface board (EIB-16; Neuralynx) with gold pins (Neuralynx) and wound them into four tetrode bundles. These bundles were then threaded through protective plastic tubing (16-mm length, 0.02 inches inner diameter, 0.002 inches wall thickness; Small Parts), attached to the EIB with Loctite Epoxy (1324007, McMaster-Carr). The plastic housing for the mechanical drive was designed in SolidWorks 2007 (Dassault Systèmes SolidWorks) and machined in-house (black Delrin, McMaster-Carr). A stainless steel thumbnut (95150A110, McMaster-Carr) was fixed to the housing with two plastic interference pins (98703A500, McMaster-Carr). The bottom half of a stainless steel vented screw (93235A081, McMaster-Carr) was thinned down from two sides to produce a 0.0625 inches × 0.086 inches cross section (original screw diameter was 0.086 inches), which resulted in an interference fit (friction fit) to the guiding tunnel of the plastic housing (0.23 inches long, 0.063 inches × 0.09 inches cross section). The vented screw was then screwed into the thumbnut and lowered by turning the thumbnut counterclockwise so that the thinned part of the screw was in the guiding tunnel, which prevented the screw from rotating during advancement. The EIB with the attached tubing and tetrode bundles was then assembled together with the mechanical drive such that EIB was flush against the vented screw cap and the protective tubing containing the tetrodes was inside the vent of the screw. A fiber ferrule (200-µm silica-core fiber, stainless steel ferrule, 5 mm tall, 2.5 or 1.25 mm in diameter, Doric Lenses) was then added to the assembly such that the optical fiber shared the inside of the protective plastic tubing with the tetrode bundles and the ferrule was set on top of the EIB for easy access. The fiber ferrule and the EIB were attached to the vented screw with Loctite Epoxy. Tetrodes were cut to the desired length (extending ~0.5 mm below the optical fiber). Colloidal gold (Neuralynx) was electrochemically deposited onto the working end of the microwires (driving current ~50 mA). This process lowered the impedance of the microwires from 3–10 MΩ to 150–350 kΩ (working impedance). The top part of the EIB was then covered in a protective layer of the Loctite Epoxy to safeguard the fragile microwires from potential damage during surgery and animal behavior (see **Supplementary Note**).

Subjects. All experiments were performed according to protocols approved by the Stanford Institutional Animal Care and Use Committee, and every precaution was taken to minimize stress and the number of animals used. We used male mice that were 8 weeks old at the time of viral injection.

Combined virus injection and optetrode implantation surgery. Genetic material for ChR2-EYFP and eNpHR3.0-EYFP was delivered to the mouse neurons using AAV5 under the control of either the *hSyn* or *CaMKIIα* promoters for wild-type mice (Jackson Laboratories) or using a DIO construct[13] with *EF1α* promoter in *PV::Cre* (S. Arber, University of Basel) transgenic mice. AAV5 virus was produced by the University of North Carolina Chapel Hill Vector Core at a titer of 3.0×10^{12} cfu ml^{-1}. All mice were anesthetized via intraperitoneal injection of ketamine-xylazine mixture before being placed into a stereotactic frame (David Kopf Instruments); a low dose of isoflurane was then provided to maintain a deep anesthetized state over the course of the surgery. Virus was injected (Nanofil syringe, World Precision Instruments) into the mPFC at three depths (1.6–1.8 mm, 2.4–2.5 mm and 3–3.3 mm from bregma). The total virus volume per injection site was 300 nl, at an injection speed of 150 nl min^{-1}. The optetrode was then lowered into the craniotomy until the tetrodes reached depths of 1.2–1.6 mm from bregma. Prior to the permanent attachment of the optetrode to the skull with Metabond (Parkell), tetrodes were protected with layers of petroleum jelly (H&H Labs) and Kwik-Kast silicone elastomer (World Precision Instruments). After implantation, the skin around the optetrode was glued together with Vetbond adhesive (3M); animals were injected subcutaneously with Buprenex (0.05 mg per kg of body weight) and Carprofen (5 mg per kg) for pain management during recovery.

Immunohistochemistry and imaging. Mice were anesthetized with Beuthanasia-D (Schering-Plough) and transcardially perfused with ice-cold 4% paraformaldehyde (wt/vol) in phosphate-buffered saline (PBS) (pH 7.4). Brains were fixed overnight in 4% paraformaldehyde and equilibrated in 30% sucrose (wt/vol) in PBS. We cut 40-µm coronal sections on a freezing microtome (Leica) and stored them in cryoprotectant (25% glycerol (vol/vol), 30% ethylene glycol (vol/vol), in PBS) at 4 °C until we processed them for immunohistochemistry. Free-floating sections were washed in PBS and then incubated for 30 min in 0.1% Triton X-100 (vol/vol) and 3% normal donkey serum (vol/vol). Slices were incubated overnight with primary antibody in 3% normal donkey serum (mouse antibody to CaMKIIα, 1:500, Abcam; rabbit antibody to parvalbumin, 1:500, Abcam; Rabbit antibody to GABA, 1:500, Millipore). Sections were then washed with PBS and incubated for 3 h at 20 °C with secondary antibodies (donkey antibody to mouse conjugated to either Cy3 or Cy5, and donkey antibody to rabbit conjugated to either Cy3 or Cy5, all at 1:1,000, Jackson Laboratories). Slices were then washed with PBS, incubated with DAPI (1:50,000) for 20 min, washed with PBS again, and mounted on slides with PVA-Dabco (Sigma). Confocal fluorescence images were acquired on a scanning laser microscope (Leica SP5) using a 40×, 1.25 NA oil-immersion objective. Images were not subjected to digital contrast or brightness adjustment.

A cohort of five mice (2 *CaMKIIα::ChR2*, 1 *CaMKIIα::EYFP* and 2 *PV::Cre*) exposed to eight stimulation epochs (30 s each) of 100 mW mm^{-2} blue light with 5-ms pulse width were processed for possible gross tissue damage; brains were fixed, sliced, DAPI stained and carefully examined. Although this blue-light treatment was, if anything, more severe than in the cases for which optogenetic stimulation was delivered in the figures, we nevertheless did not observe differences in tissue quality (deformation, altered DAPI staining or coloration, cell number, nuclear size or shape changes) below the fiber or in the neighboring tissue. Nevertheless, this is an important parameter to be tracked and examined in the course of all optogenetic experiments.

Data acquisition and analysis. All electrophysiological recordings were performed in awake freely moving animals using the Digital Lynx 10S-Z800 integrated hardware and software system (Neuralynx). The electrical signal was filtered (600–6,000 Hz) and amplified using a HS-18-CNR-LED head-stage amplifier (Neuralynx). The mouse position inside the 40 × 40-cm light-gray open field was tracked using the LED tracking system incorporated into the neural data acquisition software. The fiber and the tetrodes were propagated via the mechanical drive to the recording site at least 30 min before the experiment (and often left overnight) to ensure stable recordings. Optical stimulation was applied through a ferrule-terminated implanted optical fiber (Doric Lenses) attached to the fiber-ferrule of the optetrode by a zirconia sleeve (Doric Lenses). For optical stimulation of the mPFC in ChR2-expressing mice, we used a blue diode pumped solid-state laser (λ = 473 nm, OEM Lasers) pulsed at 5 Hz, 20 Hz, or 130 Hz with 5-ms pulse width (or in some cases 130 Hz with 2-ms pulse width) and a power density of 60–160 mW mm^{-2} at the tip of the fiber (power output was measured through a non-implanted fiber-ferrule that was identical to the one used in the optetrode). The light power at different distances from the fiber tip was estimated as a function of both wavelength and the power of light at the fiber tip (calculation from ref. 30 was corrected for wavelength).

For mice expressing ChR2 under the *hSyn* promoter, stimulation during the OFT consisted of 30-s stimulation epochs beginning every 2 min. The stimulation frequency during the epochs cycled twice through a sequence of 5-Hz, 20-Hz or 130-Hz stimulation using 5-ms pulse widths. In mice expressing ChR2 under the control of the *CaMKIIα* promoter and mice expressing ChR2 in parvalbumin-expressing neurons, as well as for the control mice that only expressed EYFP, the order of stimulation frequency was permuted to control for sequence-specific effects. Each stimulation type was applied exactly twice over the course of the OFT. For optical stimulation of the mPFC in eNpHR3.0-expressing mice, we used a green diode-pumped solid-state laser (λ = 561 nm, CrystaLaser) in continuous wave mode and power density of 160–260 mW mm^{-2} at the tip of the fiber. The 30-s stimulation epochs were separated by 90-s rest epochs and were repeated 7–8 times over the course of the experiment.

Neural data were sorted manually using OfflineSorter 2.8.9.0 (Plexon) and analyzed in MATLAB (Version 2009b, MathWorks). The maximum and minimum voltages on each of the four tetrode channels were extracted for each spike event detected by the Digital Lynx. The spike events were clustered in this eight-dimensional feature space. Clusters of spikes that were distinguishable from the noise cluster, the cluster of spikes closest to the origin, were defined using a polygon in one or more two-dimensional projections. Clusters were defined blind to the interspike interval (ISI) distribution. Only clusters containing <0.01% of the spikes with ISI < 1 ms were considered for further examination

as candidates for single units. The quality of each cluster was then assessed using two quantitative measures: L-ratio and isolation distance[30].

Theses measures calculate how well-separated the spikes in a cluster are from other spikes recorded on the same tetrode. The L-ratio treats the cluster as a multivariate Gaussian and represents the average probability that non-cluster spikes come from that Gaussian. It has been empirically shown to be particularly indicative of the number of type II errors or missed spikes. Isolation distance estimates how distant the cluster spikes are from the other spikes recorded on the same tetrode and has been shown to be indicative of the number of type I errors or contaminating spikes. Isolation distance is undefined when there are more spikes in the cluster than not in the cluster. In these rare instances, only the L-ratio was used to assess cluster quality. Clusters that had an L-ratio less than 0.2 and an isolation distance greater than 15 in the eight-dimensional feature space were considered putative single units. Because cluster quality metrics are only comparable when computed with an equal number of dimensions, tetrodes in which one or more electrodes were broken were excluded. Clusters were also examined as a function of time. During high-frequency stimulation, some clusters could be observed shifting smoothly toward lower amplitude spikes. In these cases, if the cluster remained distinguishable from other spikes, the polygon was defined to include the smeared cluster. In **Figure 3h**, two neurons did not spike during light stimulation and therefore had undefined cluster quality scores. These neurons were not counted as well-isolated during light stimulation.

For certain analyses multi-unit firing rate was used. Multi-unit firing rate was computed for each tetrode as the rate of all threshold crossings in 1-s bins for **Figures 2a**,**f** and **3a**,**g**, 100-ms bins for **Figures 2g** and **3b**, and for the entire epoch for **Figure 4**. The multi-unit firing rates were averaged over the number of independent recordings (the number of the OFT experiments multiplied by the number of tetrodes that recorded voltage threshold crossings during the experiment). The shaded regions in **Figures 2a**,**f** and **3a**,**b** and the bars in the **Figure 4c** show the standard error for these averaged values described ensemble-averaged MUA.

For the analysis of the data from eNpHR3.0-expressing mice, neurons were classified as inhibited if the z score of their firing rate during the optical stimulation was <-1.3 with respect to the background firing rate (**Fig. 2c**–**e**); neurons with z score > 1.3 were classified as enhanced (**Fig. 2e**). To calculate z scores, we divided the firing rates during prestimulation epochs and light-stimulation epochs into 10-s bins and compared the resulting distribution of rates.

To assess the effect of blue light ($\lambda = 473$ nm) stimulation on the firing rate of neurons in mice expressing ChR2 in parvalbumin-positive neurons (and in EYFP controls), we compared the average firing in the 20-ms period preceding the light pulses to the average firing in 10 ms following the light pulses during 20-Hz stimulation. The significance of the firing rate change in each neuron was assessed using nonparametric bootstrapping: 1,000 simulations using randomized pulse times.

Statistical analysis of position data was conducted in MATLAB. The center of the open field was defined as greater than 10 cm from all four walls. Position was smoothed with a 0.6-s box-filter to remove noise. Velocity at each point in time was estimated using the distance traveled in the subsequent 25 video frames (~0.84 s). In **Figure 4**, P values were computed by a Bonferroni-corrected two-tailed Student's t test.

doi:10.1038/nn.2992